Cement and Concrete Research 38 (2008) 1217–1226

Contents lists available at ScienceDirect

Cement and Concrete Research

journal homepage: http://ees.elsevier.com/CEMCON/default.asp

Reactive powder based concretes: Mechanical properties, durability and hybrid use with OPC

A. Cwirzen *, V. Penttala, C. Vornanen

Helsinki University of Technology, Laboratory of Building Materials Technology, Rakentajanaukio 5, FIN-02150 Espoo, Finland

ARTICLE INFO

Article history:
Received 2 April 2007
Accepted 18 March 2008

ABSTRACT

The basic mechanical properties, frost durability and the bond strength with normal strength concretes of the ultra high strength (UHS) mortars and concretes were studied. The produced mixes had plastic or fluid-like consistency. The 28-day compressive strength varied between 170 and 202 MPa for the heat-treated specimens and between 130 and 150 MPa for the non-heat-treated specimens. The shrinkage values were two times higher for the UHS mortars in comparison with the UHS concretes. After the initial shrinkage, swelling was noticed in the UHS mortars. The lowest creep values were measured for the non-heat-treated UHS concretes. The frost-deicing salts durability of the UHS mortars and concretes appeared to be very good even despite the increased water uptake of the UHS concretes. The study of the hybrid concrete beams indicated the formation of low strength transition zone between the UHS mortar and normal strength concrete.

1. Introduction

In the early 1990s a high performance concrete (HPC) concept appeared in the building industry market. HPC was characterized by a low water to cement ratio, use of secondary binders and superplasticizers. HPC had good workability and the 28-day compressive strength of at least 60 MPa. Durability of these concretes was in most cases improved in comparison with normal strength concretes (OPC). An early effort to produce concretes having even higher compressive strength, exceeding 150 MPa at 28 day, can be dated back to the 70s and the research of Brunauer et al. [1]. The developed concretes had a water to cement ratio of 0.2 and as binders fine Portland cement was used. Potassium carbonate (0.5%) was added to control the hydration of calcium aluminates. In the 1980s Bache [2] developed the so-called DSP concrete (Densified with Small Particles). DSP contained a high addition of silica fume, new generation of superplasticizers, and strong coarse aggregates such as diabase or calcined bauxite were used. Nowadays this concrete is mass-produced by Aalborg Cement from Denmark.

In about the same time another ultra high performance cementitious materials called MDF (Macro Defect Free) was developed by Birchall et al. [3]. In this case the cement matrix was strengthened by the addition of polyvinyl alcohol (PVA) polymer. The obtained results were astonishing. The 28-day flexural strength exceeded 200 MPa and the 28-day compressive strength reached 650 MPa. The main drawback of this concrete, which eventually did not have any practical applications, was diminishing the mechanical properties after contact with water.

Nowadays, the most widely used UHPC is the so-called Reactive Powder Concrete (RPC) and its derivatives. The roots of this material go back to France and Canada where in the 90s the theoretical bases were formulated by DeLarrard et al. [4–6] who developed the so-called linear packing density model (LPDM), solid suspension model (SSM) and more recently the compressive packing model (CPM). An interesting feature of these models was the experimental determination of certain factors. The models showed that ultra high strength and very good workability can be obtained by a combination of several features. The maximum size of the aggregates should be decreased to a few hundred micrometers and high amounts of carbon-free undensified silica fume should be used. The laboratory test showed that 28-day compressive strength exceeded 200 MPa. Others presented also that application of higher temperature and/or pressures could further increase the 28-day compressive strengths to 700 MPa. One of the major drawbacks of RPC is high cement content, which usually varies between 800 and 1000 kg/m^3. Beside a negative ecological impact and cost of the product, shrinkage is increased and microcracking of the matrix can occur. Furthermore, the RPC mixes showed often a rapid loss of workability and high amount of entrapped air [7–9].

The mix proportioning of UHPC proved to be very difficult, [10]. The mixes appeared to be extremely sensitive to any variation of the chemical composition of the binders or particle size distribution of the fillers. As a result, use of the local materials is rather problematic.

The main objective of this research project was to develop the mix proportions of UHS mortars and concretes based on a straightforward and fast optimization method using simple tests. Furthermore, the research aimed to reduce the consumption of the binders and microfillers in order to lower the material costs, to improve handling and to decrease the negative environmental impact. Workability and the

* Corresponding author. Tel.: +358 50 358 5675.
E-mail address: andrzej.cwirzen@hut.fi (A. Cwirzen).

0008-8846/$ – see front matter © 2008 Elsevier Ltd. All rights reserved.
doi:10.1016/j.cemconres.2008.03.013

mechanical properties of the obtained concretes should be comparable with RPC. The secondary objective of this research was to determine the mechanical properties and durability of the produced materials. Additionally, the bond strength between the cast "wet-to-wet" UHS mortar and OPC was evaluated.

2. Experimental set-up

Three types of cements were used in this study; low heat Portland cement CEM I 42,5 N BV/SR/LA, sulfate resistant cement CEM I 42.5 N (SR) and rapid Portland cement CEMII/A-LL 42,5R. Their chemical composition is shown in Table 1.

Two types of silica fumes were used as secondary binders. The first type was an undensified amorphous silica grade 983U produced by Elkem. This grade contained more than 97% of SiO_2 and less than 0.5% of carbon. The second type was a densified gray-colored silica grade 920 from Elkem. It contained around 87% of SiO_2 and 2% of carbon. The properties of these silica powders are given in Tables 2 and 3.

In order to improve the packing density of the binder matrix additional quartz micro-fillers were used. The chemical composition of the Nilsiä, EHK and Kemiö fillers is given in Table 4. The fourth filler marked as SAD was a quartz dust collected from the industrial air filters used in the production of Kemiö quartz. The chemical composition of this filler was similar to Kemiö quartz. The particle size distribution curves of the quartz fillers are given in Fig. 1. The coarse aggregates used in this study were granite and diabase and their basic properties are given in Table 5. Polycarboxylate based superplasticizers were used in all test concretes. The mixes were produced using a 75 l pan mixer (Zyklos ZZ 75). The mixing procedure included mixing of all dry components for 1 min, addition of the entire amount of water and superplasticizer, optionally the short steel fibers produced by Baekert (Belgium) having a length of 12 mm and a diameter of 0.1 mm, were added after 4 min. The total mixing time varied significantly but usually it was between 6 and 10 min. No delayed addition of superplasticizer was applied as the preliminary testing showed no significant improvement of workability. This result can be directly attributed to the use of polycarboxylate superplasticizers which appeared to have little interference on C_3A/SO_4 reactions in comparison with earlier generation of superplasticizers [11].

The packing density which was used for mix design was determined by using a slightly modified method developed by Puntke [12]. The Puntke method allows the approximation of the packing density by the determination of the water demand of a particle system. In this method the dry materials are mixed manually in a steel vessel until a uniform mix is obtained. Thereafter, water or water with superplasticizer is added and mixed together with the dry material. In the next step the vessel is dropped repeatedly from a constant height until a visible moistening of the surface of the material is obtained. If such wetting does not occur, more water is added and the whole procedure is repeated. If the dry mix contains also cement and silica fume the superplasticizer has to be added into the mix.

Two curing procedures were applied. The first procedure included demoulding of the specimens 24 h after casting and their subsequent storage at 95% RH and 20 °C. The second procedure shown in Fig. 2 included a heat treatment at 90 °C which was followed by storage at 95% RH. The heat treatment started 24 h after casting and lasted for 48 h. This heat treatment procedure was chosen based on an extensive study whose results are described elsewhere [13].

The rheological properties of fresh concretes were evaluated by using two methods. The first is the so-called mini cone (mini flow table) method which is normally used for estimation of flow of mortars. The second method was a modified slump test. No lifting and dropping was used in the latter test and only the mix spread was measured.

Table 1
Chemical composition of the cements

Component [%]	Sulfate resistant Portland cement (SR) [%]	Low heat Portland cement (SW) [%]	Rapid Portland cement [%]
CaO	63.1	64.9	61.1
SiO_2	20.2	22.6	19
Al_2O_3	2.2	3.4	4.5
Fe_2O_3	4	4.2	2.6
MgO	2.0	0.90	3
Na_2O	0.31	0.05	0.72
SO_3	–	2.2	3.26

Table 2
Particle size statistics of the used silica fumes

Silica fume	Mean [μm]	S.D. [μm]	d_{50} [μm]
SF Elkem 983U	43.70	46.70	26.30
SF Elkem 920D	116.00	135.00	57.80

Table 3
Chemical composition of the silica fumes according to the producers

Component	Elkem Microsilica grade 920D [%]	Elkem Microsilica amorphous grade 983U [%]
SiO_2	96.6	98
C	1.2	0.38
Fe_2O_3		0.03
Al_2O_3		0.29
CaO	<1	0.2
MgO		0.09
K_2O		0.15
Na2O		0.08
P_2O_5		0.03
H_2O	0.3	0.1
Cl	<0.3	0.01
SO_3	<2	0.08
Loss on ignition [T=975 °C]	1.3	98.5
Coarse particles; >45 μm (325 mesh)		0.08
pH-value		4.5–6.5
Bulk density [kg/m^3]	640	340

Table 4
Chemical composition of quartz fillers

Component	Nilsiä/EHK [%]	Kemiö [%]
SiO_2	99.4	98.6
Al_2O_3	0.3	0.7
K_2O	0.06	0.12
Fe_2O_3	0.03	0.028
Specific gravity [g/cm^3]	2.65	2.59
Bulk density [t/m^3]	1.1	1.4
pH (10% w/w)	5.5	8.3

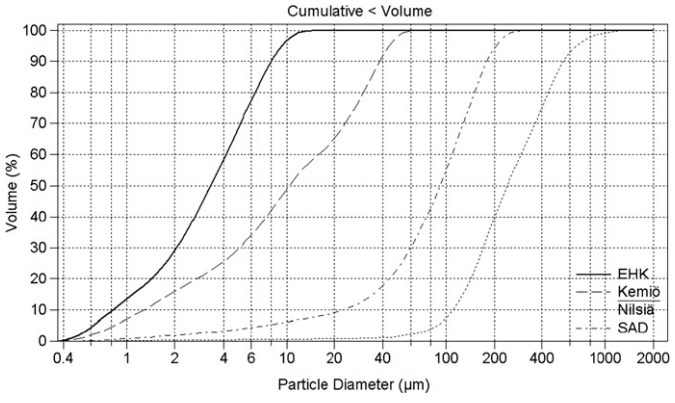

Fig. 1. Particle size distribution curves of quartz fillers.

Table 5
Aggregate fractions, densities and water absorption

Mineral type	Aggregate fractions [mm]	Density [kg/m^3]	Water absorption [%]*
Diabase	2–4, 3–6, 4–8	3085	~0.1
Granite	2–5, 5–8	2670	0.4

*water adsorption according to Scrivener and Nimeati [19].

The compressive strength was evaluated in accordance with the European standard EN 12390-3 "Testing hardened concrete—Part 3: Compressive strength of test specimens". For each measurement, a set of three specimens 10×10×10 cm^3 was used. The tests were performed at the following ages: 1, 7 and 28 days. The flexural strength was evaluated in accordance with the European standard EN 12390-5 "Testing hardened concrete—Part 5: Flexural strength of test specimens". For each measurement three beams 10×10×50 cm^3 were used. The tests were performed at the age of 28 days. The determination of the modulus of elasticity was done in accordance with a slightly modified procedure described in the Finnish standard SFS 5450. The cylindrical specimens had a diameter of 10 cm and a height of 20 cm.

Shrinkage was determined by using 200 mm high cylinders having a diameter of 50 mm. Three specimens were used for each of the studied concretes. The length changes were measured by using a mechanical dilatometer and steel studs glued to the specimens.

The creep values were determined by using similar specimens loaded axially with a load corresponding to 30% of the 7-day compressive strength. The testing equipment consisted of saucer springs, steel plates and a screw system. The shrinkage and creep measurement tests were done for a period between 2 months and 1 year, depending on the type of concrete. The shrinkage and creep specimens were moved to 65 or 85% RH 7-days after demoulding. The shrinkage measurements started 24 h after casting. 7 days after casting the creep measurements began with the load applied.

The frost durability was determined in accordance with the so-called CDF test procedure recommended by the European standards [14,15]. The specimens were cast separately and had dimensions of 70×110×150 mm^3. The test surface was cast against a teflon plate and no release oil was applied on the moulds. A 3% sodium chloride solution was used as the freezing medium. The specimens were removed from 95% RH to 65% RH at the age of 7 days where they were stored until the beginning of freeze–thaw cycles. At the age of 21 days the sealing compound was applied to the sides of the specimens. 7 days before the freeze–thaw testing started the specimens were place in a special container and subjected to the capillary suction of the freezing medium.

One freeze–thaw cycle lasted 12 h with a temperature change of ±20 °C. The tests were continued for 56 freeze–thaw cycles. Surface scaling, internal damage and water uptake were measured. The internal damage was determined by the measurements of the ultrasonic transit time.

Microstructure of the concretes was investigated by using environmental scanning electron microscope (ESEM) and mercury intrusion porosimetry (MIP). The specimens for the ESEM investigation were impregnated with resin and polished by using a diamond spray (9 to 0.25 μm). All images were taken in the backscattered electron mode (BSE) which allowed the identification of the hydration phases according to the procedure described by Scrivener [16]. The MIP core specimens had a diameter of 20 mm and a height of 25 mm and were drilled from the concrete cubes at the age of 28 days. The specimens were vacuum dried for 6 weeks prior the actual test.

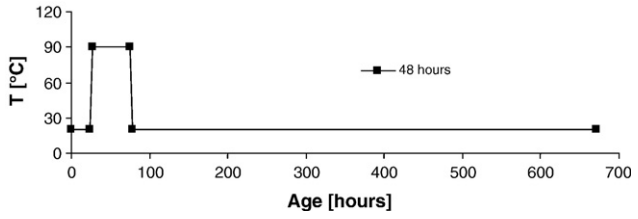

Fig. 2. Heating regime applied in the main laboratory tests.

Table 6
Mix proportions (ratios are given according to the cement weight)

Cement	Water	Super-plasticizer	Silica fume	Quartz	Sand	W/B ratio	W/C ratio
1	0.187	0.05	0.25	Variable		0.176	0.22

3. Results and discussion

3.1. Mix optimization

In order to develop the optimization criteria for the mix design procedure, a number of tests were done to establish the correlation between the water demand, wetting time, mix composition, rheological and the mechanical properties. The wetting time is considered to be the mixing time after the addition of water with superplasticizer when the mix changes from dry to moist. The mix proportions used to establish these correlations are given in Table 6.

The amount of cement, silica fume and water was fixed. Elkem 920D silica fume and sulfate resistant cement CEM I 42.5 N (SR) were used in these mixes. The mechanical properties were determined in accordance with seven and 28-day compressive strength values. The obtained results, described elsewhere [7], revealed the existence of two dependencies. The highest compressive strength of the hardened matrix corresponded to the lowest water demand of the mixture of sand and fine quartz while the highest flow value of the fresh mortar corresponded to the minimum water demand of the mortar (mix consisting of all ingredients).

After the optimum mortar mix composition was fixed, coarse aggregates could be added to the mix. The optimum composition of the mix of coarse aggregate can be derived by using the same methodology, Cwirzen and Penttala [8].

The following symbols are used to mark the different mixes; N—non-heat-treated, H—heat treatment, F—steel fibers, G—coarse granite aggregates, D—coarse diabase aggregates. The first number of the mix description denotes the dry mix name (arbitrary number) while the second denotes the water to cement ratio. For example mix F26/024/G/F/H denotes; dry mix number 26, water to cement ratio 0.24, coarse granite aggregates, short steel fibers and heat treatment.

3.2. Microstructure

The UHS mortars and concretes revealed generally dense and homogenous microstructure of the binder matrix. Examples of the BSE

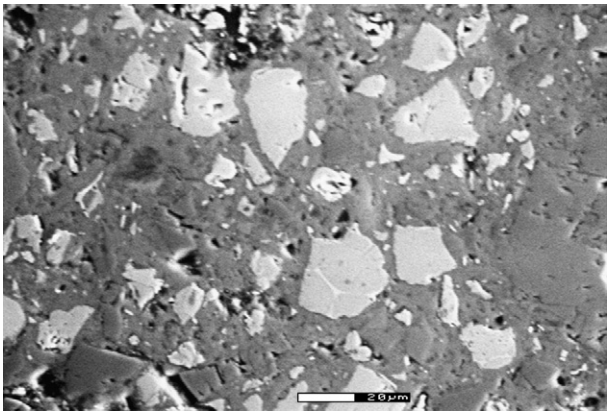

Fig. 3. Non-heat-treated specimen F26/022/N. Sand particle visible on the right side of the image.

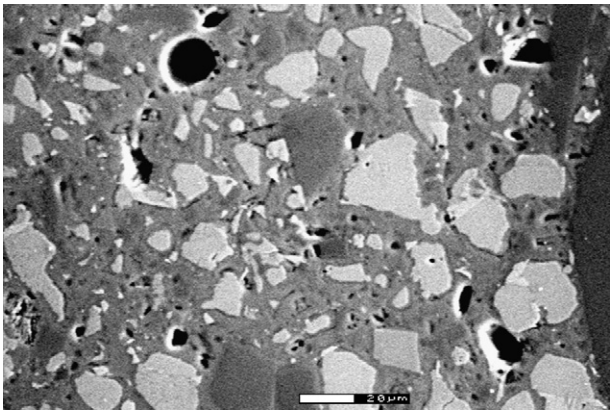

Fig. 4. Heat-treated specimen F26/022/H. Sand particle visible on the right side of the image.

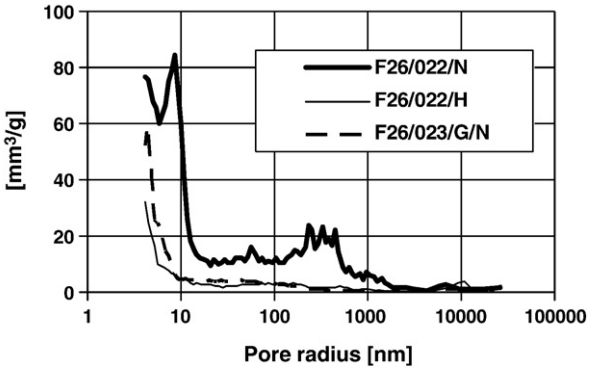

Fig. 6. MIP test results.

images of the polished samples are shown in Figs. 3–5. In general no significant difference was observed between the heat-treated and non-heat-treated specimens.

No larger agglomerates of silica fume and no significant amounts of portlandite were noticed. The MIP pore size distribution curves of the heat-treated and non-heat-treated UHS mortars and the heat-treated UHS concretes are shown in Fig. 6. The results showed that the heat treatment densified the microstructure of the binder matrix. The majority of pores had radius below 10 nm. The incorporation of coarse granite aggregates did not alter significantly the pore size distribution curves in comparison with the UHS heat-treated mortars. Furthermore, the pore size distribution curves did not indicate the existence of ITZ. Some areas of increased porosity in the vicinity of the coarse aggregate particles were revealed by the ESEM study in the case of the UHS concretes. However, since this was a random phenomenon the local microbleeding could be indicated as its main cause. Furthermore, no less anhydrous cement or more portlandite was detected near sand or coarse aggregate particles which confirms the non-existing, according to MIP and ESEM results, ITZ. In the authors' opinion the lack of the visible ITZ can be attributed to the very low water to binder ratio, very high amount of silica fume, and optimized mix design. These factors prevented the development of known mechanism creating ITZ, e.g. the wall effect or extensive microbleeding, [17–20]. The formation of portlandite was presumably hindered by fewer available in the solution Ca ions caused by pozzolanic activity of silica fume and probably also by the presence of the fine quartz fillers, [13,20].

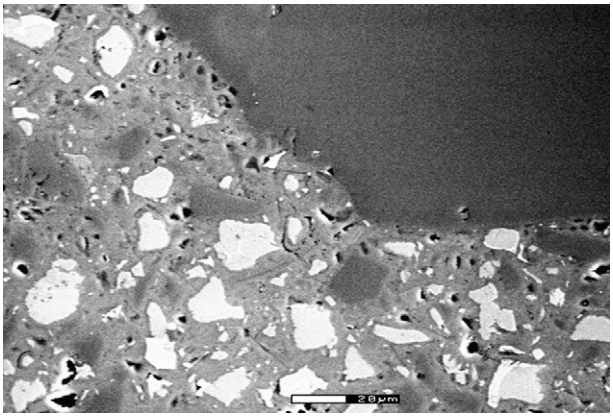

Fig. 5. Heat-treated specimen F26/022/G/H. Granite aggregate visible in the right-upper corner of the image.

3.3. Mechanical properties

The mix proportions of 33 studied UHS mortars and concretes are given in Table 7 while the mechanical properties are presented in Table 8.

The fresh concrete properties of the six main types of the studied mixes are shown in Fig. 7. The first three groups include mortars which contained fine sand or sand and quartz filler or sand, quartz filler, and steel fibers. The remaining groups incorporated additionally granite or diabase aggregates, and finally the combination of these with steel fibers.

The UHS mortars showed the wetting time between 3 and 7 min. The longest wetting time, between 6 and 7 min, was recorded in the mixes incorporating gray densified silica fume (Elkem 920). This can be attributed to a very high amount of carbon, Table 3, which, as previously described by De Larrard [4], tends to interact with the superplasticizer and thus worsens the workability of the fresh mix. The application of the undensified and characterized by a low carbon content, silica fume 983 shortened significantly the wetting time.

The UHS concretes showed, as expected, shorter wetting times which varied between 1.6 and 3 min which can be related to the improved dispersion of the materials during mixing due to the presence of the coarse aggregates. In the case of the UHS concretes only undensified silica fume, Elkem 983, was used as the preliminary tests showed a very limited flow and long wetting times when the densified Elkem 920 was applied.

The flow values measured 15 min after the end of mixing ranged from 578 mm, in the case of UHS concretes to 870 mm for the UHS mortars. However, as shown in Table 8, the water to binder ratio of the UHS concretes had to be increased to obtain workability comparable with the UHS mortars. The T_{50} time varied between 2 and 13 s. The addition of 20 and 30% of steel fibers (mixes F26/022/F and F26/022/2/F, respectively) did not worsen the rheological properties of the UHS mortars. However, in the case of the UHS concretes the presence of only 10% of steel fibers (mix F26/023/G/F) caused a decrease of the maximum flow below 770 mm and increased the T_{50} time to 6–8 s. The presence of coarse aggregates increased the tendency of the fibers to interlock between each other and the aggregate particles which worsened the workability. It followed a well known principle relating the worsening of the workability with larger maximum size of the aggregates and higher aspect ratio of the fibers, [21].

The highest measured 28-day compressive strength values for the six main groups of the heat-treated and non-heat-treated specimens are shown in Fig. 8. The highest compressive strength value of 202 MPa was obtained in the case of the heat-treated UHS mortar incorporating steel fibers. The highest compressive strength of the heat-treated UHS concretes reached 187 MPa and was measured in mix F26/026/D containing coarse diabase aggregates. The 28-day compressive strength values of the non-heat-treated UHS mortars and concretes ranged from 130 to 140 MPa.

The measured fresh mix air content was around 4% in the UHS mortars and below 2% in the UHS concretes.

Table 7
Mix proportions of the studied ultra high strength mortars and concretes

Mix	Cement amount	Cement type	Silica fume	Silica fume type	Sand (160–600 um)	Coarse aggregates			Steel fibers	Quartz fillers				SP (water+ solid)	W/C	W/B
						Diabas (3–6 mm)	Granite (2–5 mm)	Granite (5–8 mm)		Nilsä	Kemiö	EHK	SAD			
F23/022/N	1	SR	0.25	920	0.8							0.2		0.045	0.22	0.18
F23/022/H	1	SR	0.25	920	0.8							0.2		0.045	0.22	0.18
F24/022/N	1	SR	0.25	920	0.8								0.2	0.05	0.22	0.18
F24/022/H	1	SR	0.25	920	0.8								0.2	0.05	0.22	0.18
F24/022/2/N	1	SR	0.25	983	0.8								0.2	0.03	0.22	0.18
F24/022/2/H	1	SR	0.25	983	0.8								0.2	0.03	0.22	0.18
F26/022/N	1	SR	0.25	983	0.8						0.2			0.032	0.22	0.18
F26/022/H	1	SR	0.25	983	0.8						0.2			0.032	0.22	0.18
F26/022/2/N	1	SR	0.25	920	0.8						0.2			0.05	0.22	0.18
F26/022/2/H	1	SR	0.25	920	0.8						0.2			0.05	0.22	0.18
F26/022/F/H	1	SR	0.25	983	0.8				0.2		0.2			0.042	0.22	0.18
F26/022/F/N	1	SR	0.25	983	0.8				0.2		0.2			0.042	0.22	0.18
F26/022/2/F/H	1	SR	0.25	983	0.8				0.3		0.2			0.05	0.22	0.18
F26/022/2/F/N	1	SR	0.25	983	0.8						0.2			0.05	0.22	0.18
F26/022/3/H	1	SW	0.25	983	0.8									0.03	0.22	0.18
F26/022/3/N	1	SW	0.25	983	0.8									0.03	0.22	0.18
F30/022/3/H	1	SR	0.25	983	0.6					0.4				0.05	0.22	0.18
F30/022/3/H	1	SR	0.25	983	0.6					0.4				0.05	0.22	0.18
F3/022/3/H	1	SR	0.25	983	1.1									0.05	0.22	0.18
F3/022/3/N	1	SR	0.25	983	1.1									0.05	0.22	0.18
F33/022/3/H	1	SR	0.25	983	0.7						0.24		0.06	0.04	0.22	0.17
F33/022/3/N	1	SR	0.25	983	0.7						0.24		0.06	0.04	0.22	0.17
F26/023/G/F/H	1	SR	0.25	983	0.8		1		0.1		0.2			0.045	0.23	0.17
F26/024/G/F/H	1	SR	0.25	983	0.8		1		0.1		0.2			0.045	0.24	0.18
F26/023/G/H	1	SR	0.25	983	0.8		1				0.2			0.045	0.23	0.18
F26/023/G/N	1	SR	0.25	983	0.8		1				0.2			0.045	0.23	0.18
F26/023/G/2/H	1	SW	0.25	983	0.8		0.19	1.16			0.2			0.045	0.23	0.18
F26/023/G/2/N	1	SW	0.25	983	0.8		0.19	1.16			0.2			0.045	0.23	0.18
F26/024/G/3/H	1	SR	0.25	983	0.8			2			0.2			0.045	0.24	0.19
F26/024/G/3/N	1	SR	0.25	983	0.8			2			0.2			0.045	0.24	0.19
F26/026/D/H	1	SR	0.25	983	0.8	2					0.2			0.04	0.26	0.21
F26/026/D/N	1	SR	0.25	983	0.8	2					0.2			0.04	0.26	0.21

Table 8
Mechanical properties of the studied ultra high strength mortars and concretes

Mix	Compressive strength [MPa]			Flexural. 28 day [MPa]	Modulus of elasticity 28 day [MPa]	Air content [%]	Mini flow [cm]	T_{50} time [s]	Max flow after T_{50} time [cm]	"Wetting time" [min]
	1 day	7 day	28 day							
F23/022/N	67	116	146	14	41,609		30	5		6
F23/022/H	67	183	181	7	44,030		30	5		6.5
F24/022/N	64	105	127	12	40,316	5.2	20	11	630	5.83
F24/022/H	63	161	152	13	39,527	5.5	20	7	640	7.5
F24/022/2/N	64	125	142	15	42,944		30	3.5	800	3.25
F24/022/2/H	76	197	188	15	41,709	4.0	30	4	800	3.66
F26/022/N	72	125	152	15	41,575	4.0	30	3.8	785	3
F26/022/H	75	194	184	13	45,364	4.5	30	3	860	3.25
F26/022/2/N	67		137	15	45,364	5.3	20	6	665	7.5
F26/022/2/H	73	181	176	9	36,512	5.8	21.5	13	660	7.25
F26/022/F/H	64	205	202	26	45,315	3.8	30	5	820	3
F26/022/F/N	74	128	155	26	45,315	3.9	30	2	830	3
F26/022/2/F/H	61	200	202	36	45,621	4.1	30	4.7	750	3
F26/022/2/F/N	52		158	26	44,823	3.7	29	4.7	700	3
F26/022/3/H	73	174	187	15	44,106	4.0	30	2.9	820	3
F26/022/3/N	73	125	152	15	43,210	3.9	21	4	685	3
F30/022/3/H	79	116	150	14	46,829	4.2	30	2	870	3.16
F30/022/3/H	80	195	195	11	46,299	4.1	30	3.3	840	3.25
F3/022/3/H	65	176	177	12	43,191	4.2	30	2.1	870	3
F3/022/3/N	80	113	129	13	41,209	6.0	30	4.6	800	3
F33/022/3/H	76	169	189	15	43,405	4.5	30	2.3	850	3
F33/022/3/N	74	122	147	15	40,932	5.0	30	3	930	3
F26/023/G/F/H	80	180	181	14	48,095	2.4	20	8	650	2
F26/024/G/F/H	72	175	170	15	44,957	1.9	25	6	774	1.6
F26/023/G/H	73	174	167	13	47,961	2.5	25	3	850	3
F26/023/G/N	75	119	140	12	45,074	2.8	30	2	920	2.6
F26/023/G/2/H	69	170	165	13	48,205	3.2	17	8	578.5	2.8
F26/023/G/2/N	57	109	145	13	48,089	2.5	22	6	720	2.8
F26/024/G/3/H	66	178	172	13	49,554	1.7	25	7	740	2.5
F26/024/G/3/N	73	121	132	12	48,427	1.5	25	7	730	2.5
F26/026/D/H	73	187	188	15	53,107	1.2	30	5	825	2.5
F26/026/D/N	70		139	13	52,762	0.9	30	5.2	845	2.5

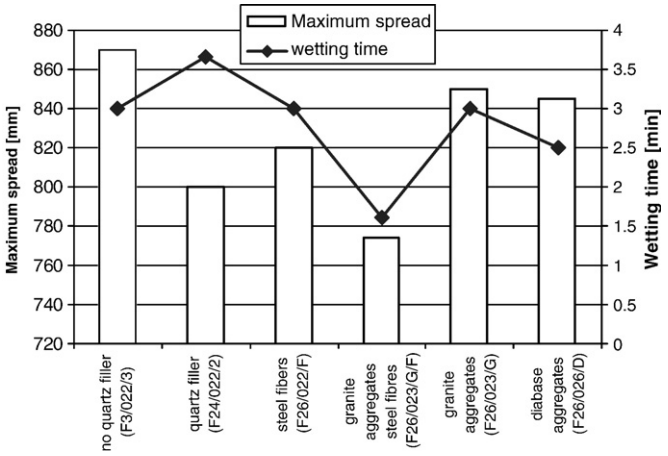

Fig. 7. Fresh concrete properties.

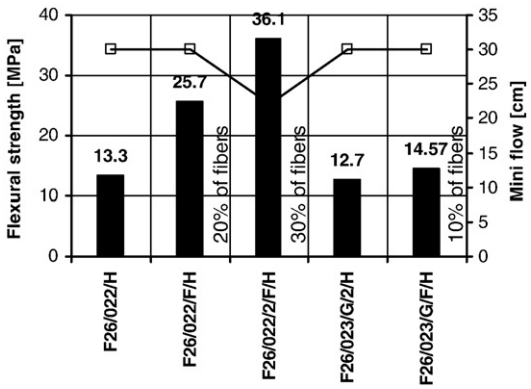

Fig. 9. Effect of steel fibers and coarse aggregates on the 28-day flexural strength.

As shown in Fig. 9, the presence of short steel fibers influenced the flexural strength of the studied mixes. The results showed an increase of the flexural strength from 13 to 25 MPa after addition of 20% of steel fibers and up to 36 MPa with 30% of steel fibers in the case of the UHS mortars. However, addition of 10% of fibers to the UHS concrete mixes resulted in only a marginal increase of the flexural strength from 12 to 14 MPa. The results showed only a very limited effect of the steel fibers on the compressive strength of the UHS mortars and negligible effect in the case of the UHS concretes. The slight enhancement of the compressive strength of the UHS mortars due to the presence of the steel fibers can be associated with the nature of the failure mechanism which is related to the tensional strength of the binder matrix.

As described by Penttala et al. [22] the tensile strength is related to the failure mechanism in tension due to the concentration of stresses at the tip of an elliptical crack. According to this theory the tensional strength will increase with shorter cracks, higher total modulus of elasticity and lower porosity. The modulus itself is influenced by three concrete phases; binder matrix, aggregates and ITZ. Consequently, the wide and porous ITZ or weak and cracked coarse aggregates will lower the tensional strength. Furthermore, the larger maximum aggregate size the greater their ultimate influence on the mechanical properties. Thus, it can be concluded that the main function of the short steel fibers is to stop the opening and the propagation of the microcracks. A negligible increase of the flexural strength of the UHS concretes after the addition of steel fibers can be explained by the unfavorable combination of at least two effects. The first effect is due to de-bonding of the binder matrix from the aggregate surface in tension. The second is due to described possible increase of the internal stresses caused by the presence of micro cracked aggregates. In order to overcome these effects significantly higher amount of the steel fibers would have to be incorporated into the binder matrix. Unfortunately, this would worsen workability of the fresh concrete.

The values of the modulus of elasticity for six main types of mixes are shown in Fig. 10. The highest value of 52 GPa was measured in the UHS concrete containing diabase aggregates. The lowest value of the modulus of elasticity which equaled slightly over 40 GPa was measured in the case of the UHS mortars. The heat treatment did not have significant effect on the measured values. In general, the modulus of elasticity increased due to the presence of coarse aggregates and depended on their type. The concretes containing granite aggregates showed lower modulus values which can be related directly to the worst mechanical properties of these aggregates in comparison with diabase.

The shrinkage and creep values are shown in Figs. 11–13. Three different mixes were produced. Two UHS mortars, F3/022 and F26/022, and one mix containing coarse granite aggregates marked as F26/024/G/3. Half of the specimens were heat-treated. The shrinkage and creep measurements were continued for 70 days in the case of the UHS concrete and for 360 days in the case of the UHS mortars. The highest shrinkage value of around 1000 μm/m was measured in the heat-treated UHS mortar without quartz filler. The UHS mortar with the addition of quartz had a shrinkage value of ~800 μm/m. In both cases, the subsequent storage at 20 °C and 65 or 95% RH caused swelling of the specimens. The ultimate shrinkage values of the UHS mortars measured after 360 days depended on the relative humidity and varied from 300 to 600 μm/m. A higher relative humidity caused lower ultimate shrinkage value. As seen in Fig. 13, the development of the shrinkage value appeared to be different for the UHS concretes. .

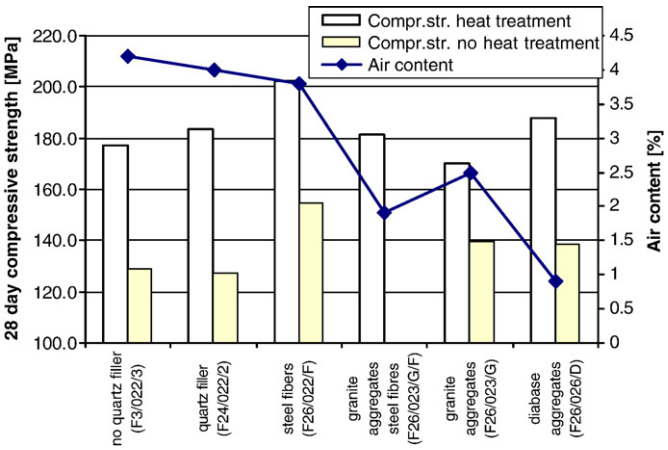

Fig. 8. The highest 28-day compressive strength values obtained in the six groups of studied concretes.

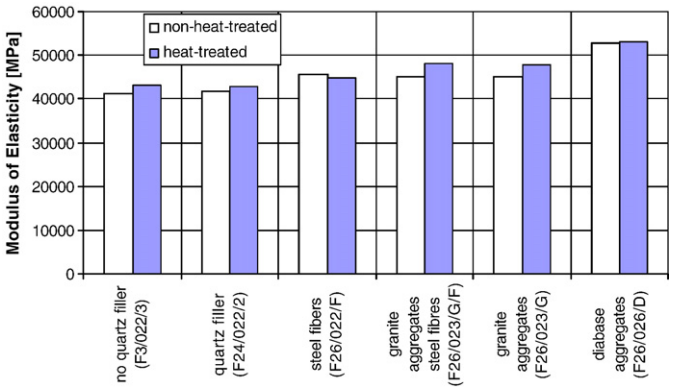

Fig. 10. Modulus of elasticity in six main groups of the studied concretes.

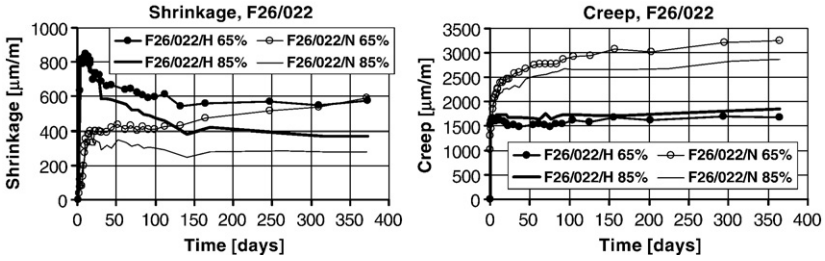

Fig. 11. Shrinkage and creep curves of UHS mortars incorporating fine quartz fillers F26/022.

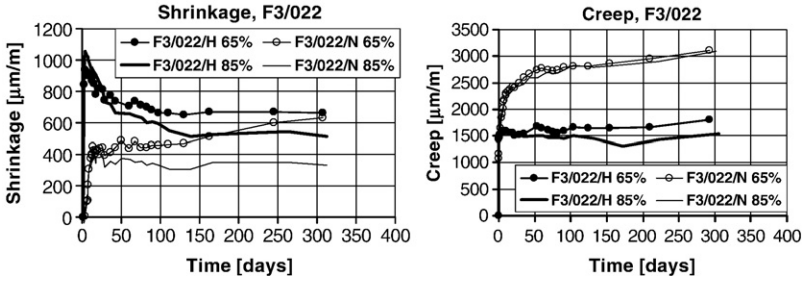

Fig. 12. Shrinkage and creep curves of UHS mortars without fine quartz fillers F3/022.

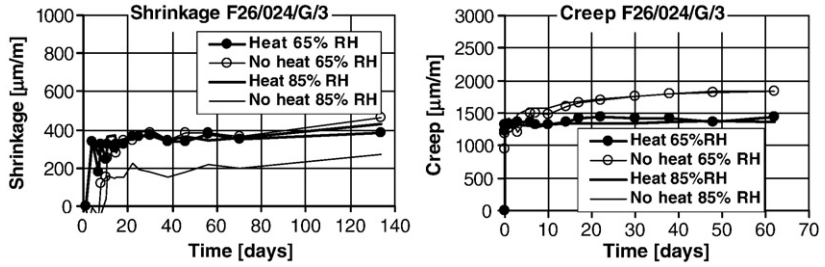

Fig. 13. Shrinkage and creep curves of mixes incorporating coarse granite F26/24/G/3, Cwirzen et al. [30].

There was no initial rapid increase of shrinkage during the heat treatment and the subsequent swelling. Instead, the majority of shrinkage developed during the heat treatment and was followed by a slight increase over the next 70 days. Furthermore, in comparison with the UHS mortar, the ultimate value was significantly lower, about only ~400 µm/m.

Also, the relative humidity appeared to have smaller effect on the measured shrinkage values. The non-heat-treated UHS mortars showed a progressive increase of the shrinkage value similarly to the UHS concretes. Higher relative humidity decreased the measured shrinkage values by 100–200 µm/m depending on the duration of the test.

However, eventually all the studied mixes showed 4–8 times higher shrinkage in comparison with OPC which does not usually exceed 40–100 µm/m, in the average.

This can be attributed to a very low porosity and low permeability of the UHS cement matrix which disrupts the ingress of water from outside and seals the interior of the specimen. The sealed conditions were indicated already by Aïtcin [23] as one of the major reason of higher shrinkage values of high performance concretes. Earlier studies by Powers and Brownyard [24] also showed that high performance concrete having a water to cement ratio of less than 0.42 is more prone to cracking caused by the self-desiccation compared with normal strength concrete, due to finer capillary porosity.

The observed decrease of the ultimate shrinkage strain values of the UHS concretes was caused by a decrease of the cement paste volume and the restraining effect of stiff granite aggregates. Soroka [25] proposed a similar effect earlier. The incorporation of coarser aggregates lowered also the shrinkage values measured in the samples stored at higher humidity. This can be explained by the presence of the interconnected network of capillary pores and locally increased porosity due to microbleeding which enhanced the water uptake of the UHS concretes [26], as observed before the freeze–thaw test, Fig. 15.

The initially high shrinkage values of the UHS mortars followed by swelling at later ages can be explained by the combination of the thermal expansion and shrinkage, see also Wittman and Lukas [27] and Kovler and Zhutovsky [28]. The thermal expansion of a cement matrix depends on the curing conditions and moisture content. Higher curing temperatures, in this case 90 °C, accelerated the hydration processes which increased the hydration shrinkage. Simultaneously,

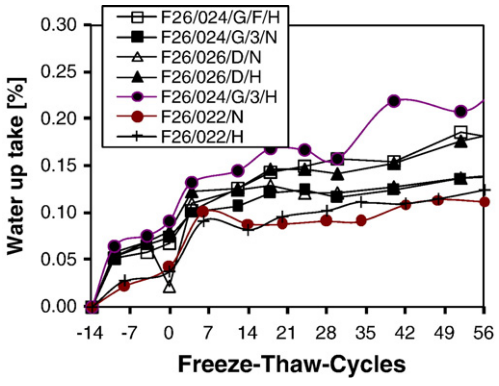

Fig. 14. Water uptake measured during freeze–thaw test.

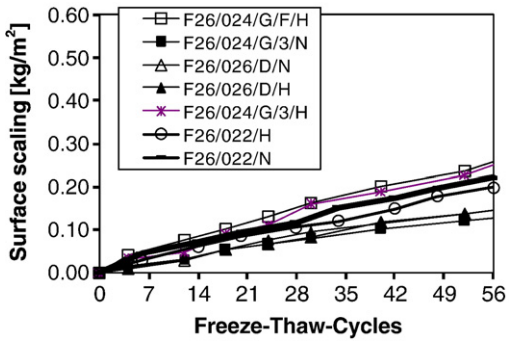

Fig. 15. Surface scaling test results.

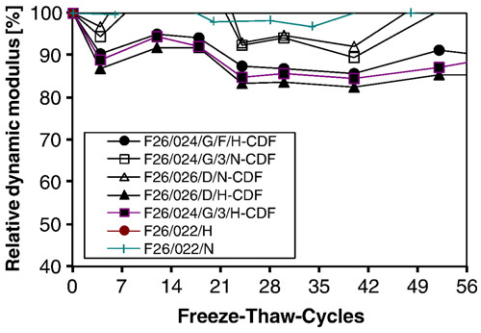

Fig. 16. Internal damage.

the thermal expansion of already hydrated binder matrix and coarse aggregates was increased. The measured shrinkage strain is a sum of these two phenomena. Another mechanism responsible for swelling, although not fully accepted, could be a disjoining (swelling) pressure which originates from the re-entry of the interlayer water between layers of CSH [29].

As expected, the incorporation of coarse aggregates decreased the measured creep values, especially concerning the non-heat-treated specimens. Relative humidity did not have any significant effect on the measured values.

3.4. Durability

The freeze–thaw test results and the measured water uptake values are shown in Figs. 14–16. As expected the measured water uptake was slightly higher in the UHS concretes. The capillary water uptake determined after 3 days of capillary suction at constant temperature and without the freeze thaw cycles, was lower in the UHS mortars in comparison with the UHS concretes, as shown in Fig. 14. All specimens were subjected to 56 freeze–thaw cycles and 3% sodium chloride solution was used as a freezing medium.

The measured surface scaling values are shown in Fig. 15. The lowest amount of the scaled material was recorded in the non-heat-treated UHS concretes; F26/026/D/N and F26/024/G/3/N. The ultimate values for these concretes were below 200 g/m^2, which fulfill the Finnish frost durability requirements of the structures having the design service life time of 200 years. All heat-treated UHS concretes and also UHS mortars, including also the non-heat-treated UHS mortars, showed the surface scaling value above 200 g/m^2.

The test revealed that after 56 freeze–thaw cycles a generally more extensive internal damage developed in the case of the heat-treated specimens. This tendency occurred in UHS mortars as well as in the UHS concretes. The damage mechanism could be directly attributed to the variation of the relative humidity within the specimen. Obviously, the heat treatment and presumably also the self-desiccation caused by a very low water to binder ratio and 25% addition of silica fume resulted in a very low internal relative humidity. The progressive water uptake into the external layer of concrete specimens and freezing of the capillary water caused increase of the relative humidity in these layers. Consequently, the ultimate difference of the relative humidity values resulted in increasing tensional stresses which exceed the strength capacity of the binder matrix and resulted in microcracking.

The specimens incorporating steel fibers revealed an increased surface scaling especially in the vicinity of the fibers located near the test surface. At the same time the presence of steel fibers lowered the internal damage which in the authors' opinion can be attributed to the crack-bridging mechanism, as described by Cwirzen and Penttala [8]. According to this mechanism the fibers bridge the forming cracks formation and hinder their further propagation and opening.

Table 9
Mix proportions of normal strength concretes

Mix	Cement	Blast furnace slag	Sand	Coarse aggregates	W/C	28 day compressive strength [MPa]
064	1	0	1.76	4.51	0.64	40
052/BFS	1	2.3	4.36	13.1	0.52	36

3.5. Hybrid concretes—bond strength

The hybrid concretes are defined here as combining UHS mortar with normal strength concrete (OPC) and being cast wet-on-wet or simultaneously. The applied tests procedure is non-standardized. The simultaneous casting was done in the case of the specimens “C” in a

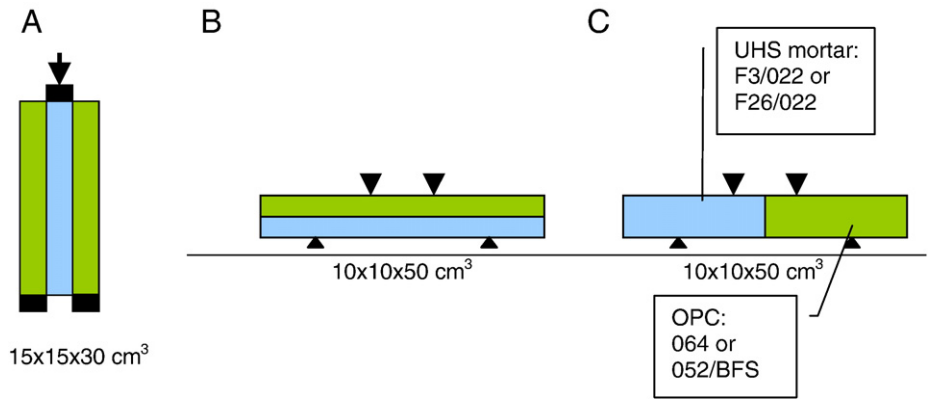

Fig. 17. Loading schemes and types of hybrid test specimens.

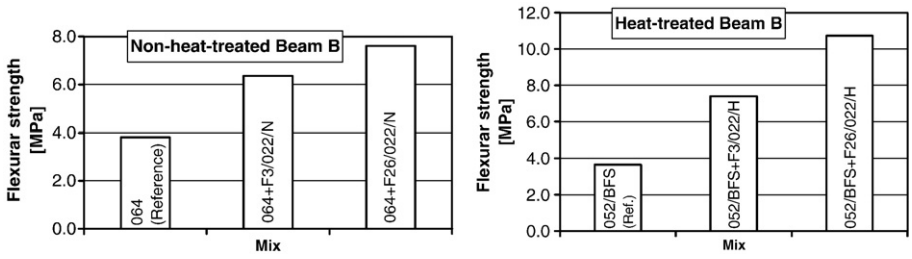

Fig. 18. The flexural strength results, hybrid beam type B.

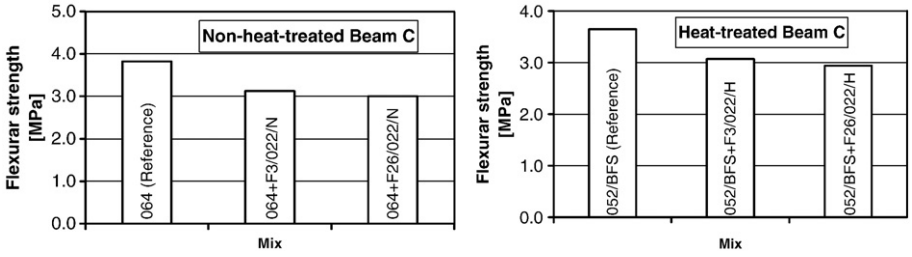

Fig. 19. The flexural strength results, hybrid beam type C.

standard 100×100×500 mm^3 steel mould which contained a temporary steel plate placed vertically in the middle, either perpendicularly to the longitudinal axis of the mould. After pouring of the two types of concretes was finished the steel plate was removed. The wet-on-wet casting was done in the case of the specimens "A" and "B" having dimensions, 150×150×300 mm^3 and 100×100×500 mm^3, respectively. In this method different concrete types were poured in layers, as shown in Fig. 17.

Due to the application of the heat treatment, one of the normal strength concretes contained 70% of blast furnace slag. The mix proportions are given in Table 9.

The applied curing procedures were the same as described previously. The bond strength and shear capacity between the OPC and the UHS mortar were determined at the age of 28 days and the results are shown in Figs. 18–20.

The results shown in Fig. 19 were obtained from the bending test of the beam type "C". The recorded strength values related to the bond strength between the OPC and UHS mortar. The hybrid concrete did break near the joint on the side of the OPC. The strength values in all cases were around 3 MPa which is nearly 1 MPa less in comparison with the reference beams made of OPC. The curing procedure had a negligible effect on the obtained results. There are two possible explanations of this result. First, weaker transition zone characterized by higher water to binder ratio and thus higher porosity could have formed between these two materials. Unfortunately, no ESEM studies of the transition zone were done. Second, higher stresses could develop in the connection zone due to different mechanical properties or different shrinkage values of the two types of concretes, see Fig. 21. The OPC concretes had an average shrinkage value of ~150 μm/m at 28 days. The UHS mortars revealed a 28-day shrinkage value of

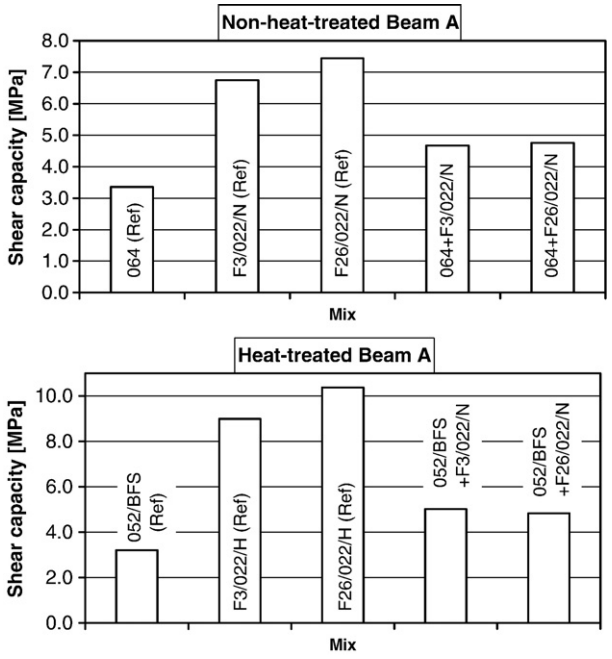

Fig. 20. The shear capacity test results, hybrid beam type A.

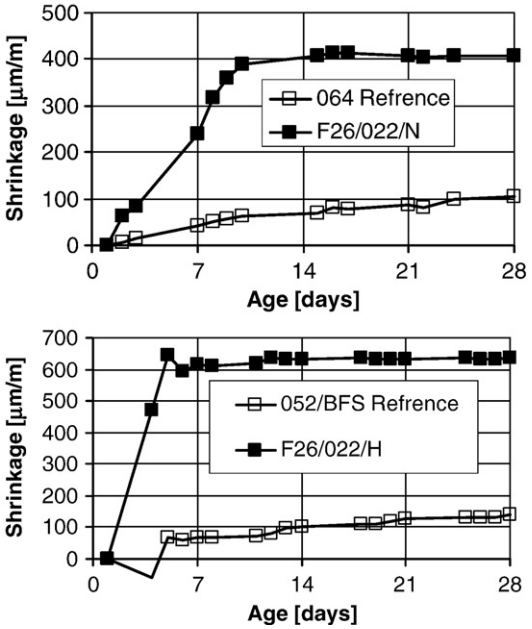

Fig. 21. Horizontal shrinkage, beams: N+F26/022/N and M+F26/022/H.

~400 μm/m and ~600 μm/m respectively for non-heat-treated and heat-treated specimens.

The shear strength values obtained for the beams type "A" are shown in Fig. 20. The recorded shear strength value for the hybrid concrete was approximately 5 MPa, regardless of the used curing procedure. This value was lower in comparison with the UHS mortars but higher than in the case of OPC.

The beam type "B", which consisted of two horizontal layers of OPC and above a layer of UHS mortar (bottom layer), see Fig. 17. The results showed that the flexural strength of the hybrid specimen value was nearly two times higher in comparison with the reference beam made of OPC. The presumably weak transition zone between the two types of concretes, as assumed on the basis of beam "C" test results, was located in the neutral zone having low stresses. As a result, the ultimate flexural strength value of the hybrid specimen increased due to higher tensional strength of the UHS mortar. This arrangement seems to be the most appropriate for the practical applications.

4. Conclusions

The presented results showed that it is feasible to produce ultra high-strength concretes applying reactive powder concretes principles and packing density theories. The 28-day compressive strength and the rheology of the UHS mortars and of the UHS concretes appeared to be comparable. The addition of steel fibers improved significantly the flexural strength only in the case of UHS mortars. Furthermore, a slightly higher water to binder ratio had to be used due to the increased water uptake of the coarse aggregates.

The addition of coarse aggregates decreased the amount of binders and improved their distribution within the binder matrix. No significant differences in the microstructure of UHS mortars and UHS concretes were detected. The handling of the UHS concretes during casting was also significantly improved in comparison with the UHS mortar. The presence of coarse aggregates lowered the measured shrinkage and creep values. In addition, there was no swelling after the initial shrinkage in the specimens produced from UHS concretes observed as in the case of UHS mortars. The water uptake of the UHS concretes was higher in comparison with the UHS mortars. It was attributed to slightly higher capillary porosity, as seen in MIP test results, and due to local microbleeding, as observed in the BSE images. The freeze–thaw cycles combined with deicing salts showed higher surface scaling and more extensive internal damage in the heat-treated specimens. The effect of the heat treatment was similar in the case of UHS mortars and concretes.

The determination of the bond strength between the UHS mortars and normal strength concretes indicated a possible formation of weaker transition zone, between these two materials. Increase of the flexural strength could be obtained in the case of the hybrid beams by placing the UHS mortar in the bottom layer and the OPC concrete on the top.

Further improvement of the mechanical properties of hybrid concretes could be achieved by, for instance, incorporation of short fibers or nano-fibers either in both concretes or only in the transition zone. In this case a more detailed study is needed.

Acknowledgments

This work is a part of a project dealing with reactive powder concretes and the financial support from Technology Development Centre of Finland—TEKES is gratefully acknowledged. We would like to thank M.Sc. Karri Mäkinen and Mr. Pertti Alho for their assistance with MIP-tests and in the production of the specimens.

References

[1] S. Brunauer, M.M. Yudenfreund, I. Odler, J. Skalny, Hardened Portland cement pasted pf low porosity, VI mechanism of the hydration processes, Cem. Concr. Res. 3 (2) (1973) 129–147.
[2] H.H. Bache, Densified cement/ultra-fine particle-based materials, Proc. International Conference on Superplasticizers in Concrete, 1981, p. 12, Ottawa.
[3] J.D. Birchall, A.J. Howard, K. Kendall, Flexural strength and porosity of cement, Nature 289 (5796) (1981) 388–390.
[4] F. De Larrard, Ultrafine particles for making of very high strength concrete, Cem. Concr. Res. 19 (2) (1988) 161–172.
[5] F. De Larrard, Concrete Mix Proportioning—A Scientific Approach, E&FN SPON, 1999 200 p.
[6] F. De Larrard, T. Sedran, Mixture proportioning of high-performance concrete, Cem. Concr. Res. 32 (11) (2002) 1699–1704.
[7] A. Cwirzen, V. Penttala, RPC mix optimization by determination of the minimum water requirement of binary and polydisperse mixtures, Proc. International Symposium on Innovation and Sustainability of Structures in Civil Engineering, Nanjing, China, 2005, pp. 2191–2202.
[8] A. Cwirzen, V. Penttala, Effect of increased aggregate size on the mechanical and rheological properties of RPC, Proceedings of Second International Symposium on Advances in Concrete through Science and Engineering, Quebec, Canada, 2006, (CD).
[9] O. Bonneau, C. Vernet, Moranville, Optimization of the rheological behavior of reactive powder concrete, Proc. 1st Int. Symp. On HPC and RPC, vol. 3, 1998, pp. 99–118, Sherbrooke, Canada.
[10] A. Cwirzen, V. Penttala, C. Vornanen, K. Junna, Self-compacting ultra high strength concrete containing coarse aggregates, TKK report, Helsinki University of Technology, Department of Civil and Environmental Engineering, Laboratory of Building Materials, 2006, No.20, 130p.
[11] N. Spiratos, M. Page, N. Mailvaganam, V.M. Malhotra, C. Jolicoeur, Superplasticizers for Concrete—Fundamentals, Technology and Practice, AGMV Marquis, Quebec, 2003 322p.
[12] W. Puntke, Wasseranspruch von feinen Kornhaufwerken, Beton 5 (2002) 242–248.
[13] A. Cwirzen, The effect of the heat-treatment regime on the properties of reactive powder concrete, Adv. Cem. Res. 19 (1) (2007) 25–33.
[14] DRAFT prEN 12390-9, Testing hardened concrete—Part 9: Freeze–thaw resistance—Scaling, (2002), p. 23.
[15] CEN/TC 51 N772, Testing the freeze–thaw resistance of concrete internal structural damage, 2003, p.26.
[16] K.L. Scrivener, P.L. Pratt, The characterization and quantification of cement and concretes microstructures, Proceedings of the First International RILEM Congress on Pores Structure and Materials Properties, Versailles, France, 1987, pp. 61–68.
[17] A. Cwirzen, Effect of the transition zone and ageing processes on the frost damage of the high strength concrete, Helsinki University of Technology, Department of Civil and Environmental Engineering, Laboratory of Building Materials, D.Sc. thesis, 2004.
[18] D. Breton, C.G. Gérard, G. Ballivy, B.J. Grandet, Contribution to the formation mechanism of the transition zone between rock-cement paste, Cem. Concr. Res. 23 (2) (1993) 335–346.
[19] K.L. Scrivener, K.M. Nimeati, The percolation of pore space in the cement paste-aggregate interfacial zone of concrete, Cem. Concr. Res. 26 (2) (1996) 35–40.
[20] H. Zanni, M. Cheyrezy, V. Maret, S. Philippot, P. Nieto, Investigation of hydration and pozzolanic reaction in reactive powder concrete (RPC) using NMR, Cem. Concr. Res. 21 (1) (1996) 93–100.
[21] ACI 544-1R-10, State-of-the-Art Report on Fiber Reinforced Concrete, ACI Committee 544; 1996.
[22] V. Penttala, P. Hannonen, M. Jarvinen, J. Komonen, Effects of aggregates and microfillers on the flexural properties of concrete, Report 5, Helsinki University of Technology, Espoo, 1995, 113 p.
[23] P.C. Aïtcin, High performance concrete, E&FN SPON, London, 1998 563 p.
[24] T.C. Powers, T.L. Brownyard, Studies of the physical properties of hardened Portland cement paste, J. Am. Concr. Inst. 22 (43) (1947) 984–987.
[25] I. Soroka, Portland Cement Paste and Concrete, The Macmillan Press Ltd., London, 1979.
[26] A. Cwirzen, V. Penttala, Aggregate-cement paste transition zone properties affecting the salt-frost damage of high performance concretes, Cem. Concr. Res. 35 (4) (2005) 671–679.
[27] F. Wittmann, J. Lukas, Experimental study of thermal expansion of hardened cement paste, Mater. Struct. 7 (4) (1974) 247–252.
[28] K. Kovler, S. Zhutovsky, Overview and future trends of shrinkage research, Mater. Struct. 39 (2006) 827–847.
[29] J.H.M. Visser, Extensile hydraulic fracturing of (saturated) porous materials, PhD thesis, (1998) Delft University.
[30] A. Cwirzen, C. Vornanen, K. Habermehl-Cwirzen, Long-term mechanical properties of low water to cement ratio ultra high strength concretes, Proc. of International Conference Concrete 07, Adelaide, Australia, 2007, p. 11, published on CD.